Surface hydrodynamics on a freely standing layer of a polymer solution

M. Hernández-Contreras,[1,*] M. W. Kim,[1,2] and P. Pincus[1]
[1]*Materials Research Laboratory, University of California, Santa Barbara, California 93106*
[2]*Department of Physics, and Advanced Materials Engineering Department, Korea Advanced Institute of Science and Technology, P.O. Box 201, Taejon 305-705, Korea*
(Received 6 January 1999)

The dispersion relation and the power spectrum of the surface modes on a surface-active, freely standing film of a concentrated polymer solution are studied with a two-component fluid model of a viscoelastic material. The diagram of bending modes is obtained from an asymptotic analysis of the dispersion equation when the bending rigidity modulus is the main elastic effect on the layer interface. The resulting dynamical structure factor provides the characteristic squeezing and undulation surface modes of the interfaces driven by thermal fluctuations or by a weak external perturbation. The effect of interfacial and bulk elastic properties on the power spectrum of the scattered light is studied. In the regime of an elastic solution, finite-thickness effects and bulk elastic properties of the layer sustain a train of elastic peaks when the wavelength of thermal fluctuations is comparable to the thickness of the layer. Interfacial elasticity properties increase the strength and shift all resonance frequency peaks producing a less intense quasielastic spectrum around zero frequency. [S1063-651X(99)03010-X]

PACS number(s): 68.35.Ja, 68.10.Et, 83.10.Dd

I. INTRODUCTION

Surface dynamics on viscoelastic films are a subject of much current interest [1–3]. They play an important role in the stability of emulsions, foams, in the process of hydrodynamic relaxation of biological membranes, as well as in other technological applications [4–6]. Modern techniques including inelastic light scattering provide accurate information about the surface hydrodynamics of polymer solutions, and measure the spectral intensity $S(k,w)$ of the scattered light, of frequency w and magnitude of wave vector k, by the interface roughness and thermal fluctuations [1]. The experimental investigation of the surface modes in clearly characterized film systems made of polyethylene oxide in water and polyisobutylene in organic solvents have posed intriguing questions concerning the effect of solvent quality, bulk shear elasticity, surface tension, and interfacial elasticity on the interfacial roughness fluctuations [2,3,7–9].

Theoretical studies of the surface dynamics on concentrated polymer solutions have mostly been based on the two-fluid model of a supported viscoelastic polymer solution in a solvent that was predicted to exhibit a crossover from capillary to viscoelastic surface fluctuations as a function of polymer concentration [10–12], a prediction that has been recently verified experimentally [2,7–9]. Moreover, this approach was later extended including the effect of interfacial elasticity on capillary and elastic Rayleigh modes [12]. The hydrodynamic modes of a very thin layer of viscoelastic materials were studied [13], finite-thickness effects on the surface modes on a freely standing viscoelastic soap film [14], and polymer gels [15] were also considered. An important class of viscoelastic polymer films that can be found at liquid-vapor interfaces includes insoluble liquid films of polymeric surfactants such as those found in amphiphilic membranes of very low-surface tension and low-bending energy [5,16,17].

The energy required in these systems to create a deforming surface wave include a corresponding restoring force due to the mean bending elastic modulus. In this paper we extend the two-fluid-model approach to include the elastic bending rigidity in the description of the surface hydrodynamics of liquid films such as it is found in amphiphilic membranes of surfactant materials. We address the problem of determining the exact dispersion relation of the surface modes due to the bending rigidity modulus, surface tension, and interfacial elasticity of a symmetric freely standing film of a viscoelastic monolayer. An asymptotic analysis of the dispersion relation provides the diagram of surface modes when the bending rigidity modulus is the only elastic parameter that determines the structure of the interfaces and the shear elastic modulus, the bulk property of the layer. The diagrams for the squeezing and undulation surface modes show a crossover from bending finite-thickness propagating modes over dissipative overdamped to elastic waves when the polymer concentration is increased. For a layer constituted by a simple Newtonian fluid with bending rigidity the maximum of the power spectrum is more enhanced than in the case of a viscoelastic layer.

We show that for a wavelength comparable to the thickness of the viscoelastic layer, in the absence of a bending rigidity modulus and far into the elastic regime, bulk shear elasticity sustains a series of peaks in the power spectrum. Low wave vectors tend to merge these peaks into a single broad peak. This spectral property may be observed by the present light-scattering techniques in a sufficiently concentrated layer of viscoelastic material. In the next section we introduce the viscoelastic layer model. The hydrodynamic theory of the thermal fluctuations at the interfaces is given in Sec. III. The relevant hydrodynamic modes of the thermal

*Also at Departamento de Física, Centro de Investigación y Estudios Avanzados del IPN, Apartado. Postal 14-740, México D.F., Mexico.

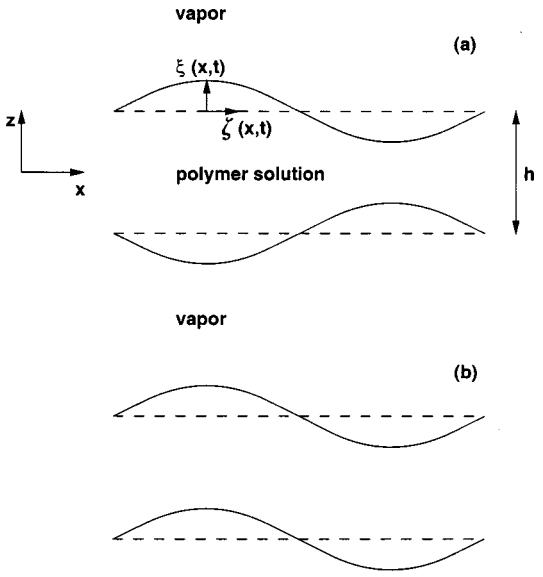

FIG. 1. Geometry of a symmetric viscoelastic polymer layer of thickness h. The equilibrium interface configurations correspond to the dashed lines. (a) Squeezing and (b) undulatory modes.

fluctuations and power spectrum are given in Sec. IV and the physical description of them is given in Sec. V. Section VI is a brief summary.

II. MODEL POLYMER FILM

Figure 1 shows our model of a viscoelastic layer that consists of two infinite interfaces in the X and Y directions that are separated by a mean distance h. We assume that the interfaces are identical and contain a polymer solution in contact with a vapor in a symmetric 1-1 electrolyte solution of monovalent ions of charge $\pm e$ released in the solvent of a dielectric constant ϵ_s at concentration n. Since there is symmetry in the XY plane we assume the fluctuations are independent of the coordinate Y and take the surface wave propagating with wave vector $\mathbf{k}$ in the X direction. We denote by $\xi(x,t)$ and $\zeta(x,t)$ the shape of the interface in the normal and lateral displacements from its equilibrium configuration at time t. We think of the two interfaces as charged elastic membranes with adsorbed ions or ionic amphiphilic molecules that provide an interfacial elasticity ϵ with the surface tension γ, and the curvature elastic deformation energy K determines the equilibrium shape configuration of the interface.

In thermodynamic equilibrium, the thickness of a layer results from a balance of the direct interactions between the interfaces as given by the repulsive electrostatic double-layer forces of the membranes and the conventional, nonretarded, attractive Van der Waals interaction $W_d = -H(6\pi h^3)^{-1}$, where H is the Hamaker constant for water-hydrocarbon contact typically having the value 6×10^{-21} J. Thus, the force is approximately given by

$$P_d(h) = 64 k_B T n A_1 e^{-\kappa h} + W_d . \tag{1}$$

Here the first term accounts for the electrostatic interaction of two flat and weakly overlapping double layers; the range of interaction is given by the inverse Debye length $\kappa = \sqrt{8\pi I n}$ where $I = e^2/\epsilon_s k_B T$ is the Bjerrum length with k_B the Boltzmann constant and T the temperature. In Eq. (1), A_1 is a function of the surface potential ψ_0 given by $\tanh(e\psi_0/4k_BT)$. On the other side, the elastic properties of a surface are given by the viscoelastic free energy of an interface deformation that has three contributions,

$$F = \frac{1}{2}\int_a K\left(\frac{\partial^2\xi}{\partial x^2}+\frac{\partial^2\xi}{\partial y^2}\right)^2 dS + \frac{1}{2}\int_a \gamma\left[\left(\frac{\partial\xi}{\partial x}\right)^2+\left(\frac{\partial\xi}{\partial y}\right)^2\right]^2 dS + \frac{1}{2}\int_a \epsilon\left[\left(\frac{\partial\zeta}{\partial x}\right)^2+\left(\frac{\partial\zeta}{\partial y}\right)^2\right]^2 dS. \tag{2}$$

The first term in Eq. (2) is the curvature free energy of an elastic membrane with rigidity K, and the second term describes the coupling of a change in unit area a of deformation with a corresponding change in volume [18]. Both terms determine the strength of the deformation of the interface due to fluctuations in the vertical positions of the adsorbed molecules. The third term is the free energy associated with fluctuations of the position of molecules in the plane of the interface with interfacial elasticity modulus ϵ, which is related to the concentration of adsorbed material [19].

III. EQUATIONS OF MOTION AND BOUNDARY CONDITIONS

In this section we quote the main results of the two-coupled fluid-model approach for the description of the hydrodynamics of the surface wave of a viscoelastic medium of a polymeric material. The equations of motion of the velocity field $\mathbf{v}$ of the fluid and the displacement field $\mathbf{u}$ of the polymer [4,21] can be written in the form

$$\rho_s\frac{\partial\mathbf{v}}{\partial t} = \boldsymbol{\nabla}\cdot(\boldsymbol{\sigma}^{(s)}+M) - \rho_s\boldsymbol{\nabla}W + \mathbf{f}_I(\mathbf{v},\dot{\mathbf{u}}),$$

$$\rho_p\frac{\partial^2\mathbf{u}}{\partial t^2} = \boldsymbol{\nabla}\cdot(\boldsymbol{\sigma}^{(p)}+M) - \rho_p\boldsymbol{\nabla}W - \mathbf{f}_I(\mathbf{v},\dot{\mathbf{u}}). \tag{3}$$

ρ_s and ρ_p denote the solvent and polymer densities, $\boldsymbol{\sigma}^{(s)}$ and $\boldsymbol{\sigma}^{(p)}$ are the local solvent and polymer stress tensors, and $\mathbf{f}_I = C_1(\dot{\mathbf{u}}-\mathbf{v})$ is the local polymer-solvent coupling term. The proportionality constant scales as $C_1 = \eta_s/l$, where l is the mesh size of the polymer network and η_s is the solvent shear viscosity. On the other hand, the strain tensors are given by [22],

$$\boldsymbol{\sigma}^{(s)}_{ij} = \eta_s\left(\frac{\partial v_i}{\partial x_j}+\frac{\partial v_j}{\partial x_i}\right) - p_s\delta_{ij},$$

$$\boldsymbol{\sigma}^{(p)}_{ij} = E(t)\left(\frac{\partial u_i}{\partial x_j}+\frac{\partial u_j}{\partial x_i}\right) + \left(F(t)-\frac{2}{3}E(t)\right)[\boldsymbol{\nabla}\cdot\mathbf{u}]\delta_{ij}. \tag{4}$$

p_s is the solvent hydrostatic pressure, v_i is the ith component of the solvent velocity field, $E(t)$ and $F(t)$ denote the complex shear and compressional moduli of the polymer network, and u_i is the ith component of the polymer network displacement field. The direct interactions are embodied in the Maxwell stress tensor $M(x,z,t)$ and the Van der Waals

potential $W(x,z,t)$ [4,14]. The contribution $W(x,z,t)$ is the sum of all long-range Van der Waals interactions between all particles in the fluid and between the particles in the interface with others in the solution. Following the procedure of Ref. [4] we can formulate Eq. (3) in a different manner.

In the infinite coupling limit, $\mathbf{v}\rightarrow\dot{\mathbf{u}}$, the Fourier and Laplace transform of Eq. (3) reduces to an effective equation of motion,

$$iw\rho\mathbf{v}=\boldsymbol{\nabla}\cdot\boldsymbol{\sigma}(w), \tag{5}$$

where now

$$\boldsymbol{\sigma}_{ij}(w)=\eta(w)\left(\frac{\partial v_i}{\partial x_j}+\frac{\partial v_j}{\partial x_i}\right)-P(w)\,\delta_{ij}, \tag{6}$$

$\rho=\rho_s+\rho_p$, $i=\sqrt{-1}$,

$$\eta(w)=\eta_s+E(w)/iw, \tag{7}$$

and

$$P(w)=p_s(w)-[F(w)-\tfrac{2}{3}E(w)][\boldsymbol{\nabla}\cdot\mathbf{v}(w)]/iw+P_{\mathbf{eff}}. \tag{8}$$

Due to the high compressibility modulus of the polymer network, the second contribution to $P(w)$ in the last equation, Eq. (8), is small compared to $p_s(w)$. Therefore, it will be neglected in the subsequent expressions. The third term on the right-hand side of Equation (8), $P_{\mathbf{eff}}$, is the effective pressure contribution due to the direct interactions between the two interfaces and is determined in [4]. Its specific form enters only through the boundary conditions that the velocity field $\mathbf{v}$ satisfies at the interfaces and will be provided below. Since we are assuming that the speed of propagation of the surface wave is small compared to the speed of sound, Eq. (5), it should also be complemented with the imcompressible fluid condition

$$\boldsymbol{\nabla}\cdot\mathbf{v}=0. \tag{9}$$

Equations (5) and (9) provide the hydrodynamic description of the surface modes in terms of the velocity field $\mathbf{v}$ that is subject to the boundary conditions at the free interfaces. Using Eqs. (1) and (2), one can write for the effective force per unit area in the normal direction to the membrane [4,20]

$$p^0=p_s+\gamma\frac{\partial^2\xi}{\partial x^2}+K\frac{\partial^4\xi}{\partial x^4}-P_d'(h)\,\delta\xi+2\,\eta\frac{\partial v_z}{\partial z}, \tag{10}$$

where $P_d'(h)\equiv dP_d(h)/dh$, $\delta\xi$ is the thickness of the layer, and $p^0=\Pi^0 e^{i(kx+wt)}$, a weakly applied external perturbation of constant strength Π^0. A surface-active material on the liquid interfaces implies the existence of in-plane tangential stress, which satisfies the following boundary condition:

$$\boldsymbol{\sigma}_{zx}=\epsilon\frac{\partial^2\zeta}{\partial x^2},\quad z=\pm\frac{h}{2}, \tag{11}$$

where ϵ is the interfacial elasticity of the membrane. The normal coordinate to the interface is represented by $z=h/2+\xi(x,y,t)$, where ξ is small compared to $h/2$. $\xi(t)$ and $\zeta(t)$ are related, respectively, to the local profile velocity components as $\dot{\xi}_{I,II}(t)\approx v_z(x,z=\pm h/2,t)$ and $\dot{\zeta}(t)\approx v_x(x,z=\pm h/2,t)$.

The most general solution of Eqs. (5) and (9) is a stationary wave that satisfies the asymptotic limit $\mathbf{v}(w)\rightarrow 0$ as $z\rightarrow\pm\infty$ and has the form [23]

$$\begin{aligned}
v_x&=\{ik[A\sinh(kz)+B\cosh(kz)]\\
&\quad -q[C\cosh(qz)+D\sinh(qz)]\}e^{i(kx+wt)},\\
v_z&=k\{A\cosh(kz)+B\sinh(kz)\\
&\quad +i[C\sinh(qz)+D\cosh(qz)]\}e^{i(kx+wt)}\\
p_s&=-iw\rho[A\sinh(kz)+B\cosh(kz)]e^{i(kx+wt)},
\end{aligned} \tag{12}$$

where the constants A,B,C,D, and the value of the wave vector q should be determined from the above given boundary conditions, Eqs. (10) and (11).

The thermal waves described by Eq. (12) embody two types of a liquid motion. One may observe that the interfaces move out of phase in the normal direction $\hat{\mathbf{z}}$ to the layer, so that the components satisfy $v_z(x,z,t)=-v_z(x,-z,t)$ and $v_x(x,z,t)=v_x(x,-z,t)$. This is called the squeezing relaxation mode. On the other hand, when the two interfaces move parallel to the normal direction so that $v_z(x,z,t)=v_z(x,-z,t)$ and $v_x(x,z,t)=-v_x(x,-z,t)$ one encounters the so-called undulatory mode. From now on, superscript letters ''s'' and ''u'' denote the squeezing and the undulatory mode, respectively. The above-displayed parity properties of the velocity components with respect to coordinate z allow one to study separately each of the two relaxation dynamics of a liquid motion on the layer.

IV. POWER SPECTRUM OF SQUEEZING AND UNDULATORY MODES

The application of a weak external pressure $p^0(x,y,t)\hat{\mathbf{z}}$ on the interface contribute to the deformation energy of the surface as $-\int_a\xi(x,y,t)p^0(x,y,t)dS$. Therefore, at first order in $p^0(x,y,t)$ linear-response theory [1] allows us to find the general form of the interface deformation in the normal direction, namely,

$$\xi(x,t)=\int_a\int_0^\infty\chi(x-x',y-y',\tau)p^0(x',y',t-\tau)d\tau dS'. \tag{13}$$

The Fourier and Laplace transformed response function $\chi(k,w)$ is related to the surface displacement autocorrelation function $\langle\xi(k,t)\xi(k,0)\rangle$ through the fluctuation-dissipation theorem, which provides the exact expression of the power spectrum $S(k,w)$ of the scattered light

$$S(k,w)=\frac{k_BT}{\pi w}\mathrm{Im}[\chi]. \tag{14}$$

The relaxation function χ is related to both dynamical modes discussed above through the amplitudes of the thickness variation of a polymer film, i.e.,

$$\delta\xi^s=\chi^s\Pi^0=\tfrac{1}{2}(\xi_I-\xi_{II})$$

$$\delta\xi^u=\chi^u\Pi^0=\tfrac{1}{2}(\xi_I+\xi_{II}). \tag{15}$$

We will describe briefly the procedure to determine the response functions χ^s and χ^u that are involved in the exact expression of the power spectrum $S(k,w)$ for the symmetric layer case. We have seen above that for the squeezing mode $A=D=0$ and, therefore, C and B should have a finite value. Thus, we replace the velocity components of Eq. (12) in the boundary conditions as given by Eqs. (10) and (11) from which we obtain two equations for the two unknown constants, C and B, in terms of the strength Π^0 of the weakly applied external perturbation. We find

$$B=\frac{-\Pi^0 w^2}{D^s(k,w)}\left[-n(q^2+k^2)\sinh\left(\frac{qh}{2}\right)+\epsilon\frac{k^2q}{iw}\cosh\left(\frac{qh}{2}\right)\right],$$

$$C=\frac{\Pi^0 w^2}{D^s(k,w)}\left[2nik^2\sinh\left(\frac{qh}{2}\right)-\epsilon\frac{k^3}{w}\cosh\left(\frac{hk}{2}\right)\right], \tag{16}$$

and

$$D^s(k,w)=[-w^2+2i\nu(w)k^2w]^2-w^2\left[w_a^2+\frac{\epsilon}{\rho}qk^2\coth\left(\frac{hq}{2}\right)-4\nu(w)^2k^3q\tanh\left(\frac{hk}{2}\right)\coth\left(\frac{hq}{2}\right)\right]+\frac{\epsilon k^2w_a^2}{\rho}\left[q\coth\left(\frac{hq}{2}\right)-k\coth\left(\frac{hk}{2}\right)\right], \tag{17}$$

$$w_a^2=\tanh\left(\frac{hk}{2}\right)w_c^2,$$

$$w_c^2=[\gamma k^3+Kk^5-2kP_d'(h)]\frac{1}{\rho}, \tag{18}$$

$$q^2=k^2+\frac{iw}{\nu(w)}, \tag{19}$$

with $\nu(w)=\eta(w)/\rho$. The function $D^s(k,w)$ is the dispersion relation of the squeezing mode as given by the two-fluid model of a viscoelastic material. The viscoelastic properties of the polymer solution are set in terms of the complex frequency-dependent shear viscosity $\eta(w)$. Equation (17) corresponds to the dispersion relation of capillary waves in a Newtonian liquid [22] having the viscosity η_s. A simple model for the complex shear viscocity is the Maxwell model of a single chain relaxation time τ of entanglements [$\eta(w)=\eta_s+E\tau/(1+iw\tau)$], which predicts a crossover from an interfacial capillary wave mode at low bulk-volume concentrations of a polymer solution to a viscoelastic dissipative mode at high concentration [10]. Recently, these predictions of the two-fluid model have been proved experimentally for a very thin polymer film [7–9]. These experimental findings and the theoretical analysis [10–13] correspond to the limit $h\to\infty$ of a single fluctuating monolayer in this context of a finite thickness layer model.

The power spectrum is determined once we find χ^s. We now use the results of B and C of Eq. (16) in Eq. (15) for χ^s from which we get

$$\chi^s=\frac{k\tanh\left(\frac{hk}{2}\right)}{\rho D^s(k,w)}\left\{-\frac{\epsilon k^2}{\rho}\left[q\coth\left(\frac{hq}{2}\right)-k\coth\left(\frac{hk}{2}\right)\right]+w^2\right\}. \tag{20}$$

For the undulatory mode we need to consider now the case $B=C=0$ in order to satisfy the symmetry requirements on the components of the velocity when changing the sign of the coordinate z. Using similar methods we obtain the relaxation function of the undulatory mode,

$$\chi^u=\frac{k\coth\left(\frac{hk}{2}\right)}{\rho D^u(k,w)}\left\{-\frac{\epsilon k^2}{\rho}\left[q\tanh\left(\frac{hq}{2}\right)-k\tanh\left(\frac{hk}{2}\right)\right]+w^2\right\}, \tag{21}$$

where the dispersion relation is now given by

$$D^u(k,w)=[-w^2+2i\nu(w)k^2w]^2-w^2\left[w_b^2+\frac{\epsilon}{\rho}qk^2\tanh\left(\frac{hq}{2}\right)-4\nu(w)^2k^3q\coth\left(\frac{hk}{2}\right)\tanh\left(\frac{hq}{2}\right)\right]+\frac{\epsilon k^2w_b^2}{\rho}\left[q\tanh\left(\frac{hq}{2}\right)-k\tanh\left(\frac{hk}{2}\right)\right], \tag{22}$$

$$w_b^2=\coth\left(\frac{hk}{2}\right)w_c^2. \tag{23}$$

In the undulatory mode-dispersion relation Eq. (22), the disjoining pressure plays no role, which follows from the fact that in this case there is no thickness variation and hence no coupling to the direct interaction. Both Eqs. (17) and (22) are equivalent to the dispersion relations of Joosten [20] when $K=0$, and the complex shear viscosity $\eta(w)$ is replaced by a real constant value η_s in order to conform to his model of a surface-active, but finite-thickness soap film in a Newtonian solvent with viscosity η_s. Therefore, our results in Eqs. (17) and (22) constitute their generalization for a viscoelastic layer of a polymer solution.

The single interface limit of a semi-infinite medium is obtained from either Eqs. (17)–(19) or Eqs. (22) and (23) with $h\to\infty$; the relaxation function $\chi_{\sin}$ is given now by

$$\chi_{sin}=\frac{k}{\rho D_{\sin}(k,w)}\left[-\frac{\epsilon k^2}{\rho}(q-k)+w^2\right], \tag{24}$$

where the corresponding dispersion relation

$$D_{\sin}(k,w)=(-w^2+2i\nu k^2 w)^2-w^2\left(\frac{\gamma k^3+Kk^5}{\rho}+\frac{\epsilon q k^2}{\rho}-4\nu^2 k^3 q\right)+\frac{\epsilon k^2}{\rho}(q-k)\left[\frac{\gamma k^3+Kk^5}{\rho}\right]. \quad (25)$$

Equation (25) is a generalization of the dispersion relation of Harden *et al*. [10] (in their work, K and ϵ are zero), and of Wang and Huang [12] (case of $K=0$, see Appendix A) for a surface-active film on a semi-infinite medium of a polymer solution with a finite-bending modulus K. It also generalizes the dispersion relation of Lucassen and Lucassen-Reynders [19] for a monolayer without viscoelastic properties and elastic constants ϵ and γ (see Appendix B). Equations (20) and (21)–(24) could be relevant to the study of the interfacial hydrodynamics of a certain model of a biological membrane where surface tension is a negligible effect and for which curvature energy dictates the dynamical properties of the roughness interface thermal fluctuations [5].

V. DISCUSSION

In this section we show the diagram of surface wave regimes due to bending rigidity modulus K as the function of the magnitude of the wave vector k and shear modulus E. The next step will be the discussion of the power spectrum.

We consider the case when the surface tension γ, the interfacial elasticity ϵ, and the direct interaction, P_d, between the interfaces, are zero. The more complex situation will correspond to the case that these elastic constants have a finite value. However, when $\gamma > K/h^2$ surface tension overwhelms the bending modes and the theory outlined here reproduces the known mode phase diagram at long and short wavelength, and at low to high frequency [14]. In the case that $\gamma < K/h^2$ and $\epsilon < K/h^2, \epsilon$ and γ contribute a small effect as compared to bending rigidity. In this case we obtain a diagram of bending modes that we will describe below. In the relevant experimental long wavelength limit $hk<1$, and in the low concentrated regime, the dynamics of the surface fluctuations is determined mainly by the viscous behavior ($w\tau<1$). In this limit the Maxwell constitutive equation can be approximated by the expression of the viscosity as a function of the bulk shear elasticity $\eta(w)=E\tau+\eta_S$. The dispersion relation of the squeezing mode, Eq. (17), predicts the existence of several resonance peaks, which scale with the magnitude of the wave vector k as shown in Fig. 2(a). In region I there is a propagating thickness-dependent bending mode $w_K^2=Kk^6h/2\rho$ for a low value of the kinematic viscosity $\nu=\eta(w)/\rho$. For moderate to high wave vector, $(K/\rho\nu^2h)^{1/2}<kh<1$, there is an overdamped bending mode $w=-iKk^4/8\eta$ and a viscous solution mode $w=i4\nu k^2$, which lies in region II. For a wave vector in the range $hk<(K/\rho\nu^2h)^{1/2}<1$ there is an overdamped bending mode $w=iKk^6h^3/24\eta$. In the opposite limit of high-frequency $w\tau>1$, the kinematic viscosity is frequency-dependent and given by $\nu=\nu_s+E/iw\rho$. The dispersion relation predicts two propagating modes, a bending mode $w^2=w_K^2$, and a Rayleigh elastic wave, $w^2=4Ek^2/\rho$ (region III). The boundary line between the regions of propagating waves (I) and the dissipative modes (II) is given by $k=E(\tau^2/Kh\rho)^{1/2}$ and $E=(Kh\rho/\tau^4)^{1/2}$. The crossover between the overdamped (region II) and the elastic waves (region III) is given by $k=(\rho/E\tau^2)^{1/2}$. The separation line between waves of region I and those of region III is $k=(E/Kh)^{1/4}$. The boundary line between the Rayleigh waves (III) and the semi-infinite single interface limit bending mode (region IV) $w^2=Kk^5/\rho(kh>1)$ is given by $k=(E/K)^{1/3}$. At short wavelength $kh>1$ with a finite thickness layer there appears the overdamped mode $w=iKk^3/4\eta$ that describes the dynamics of a locally free single interface.

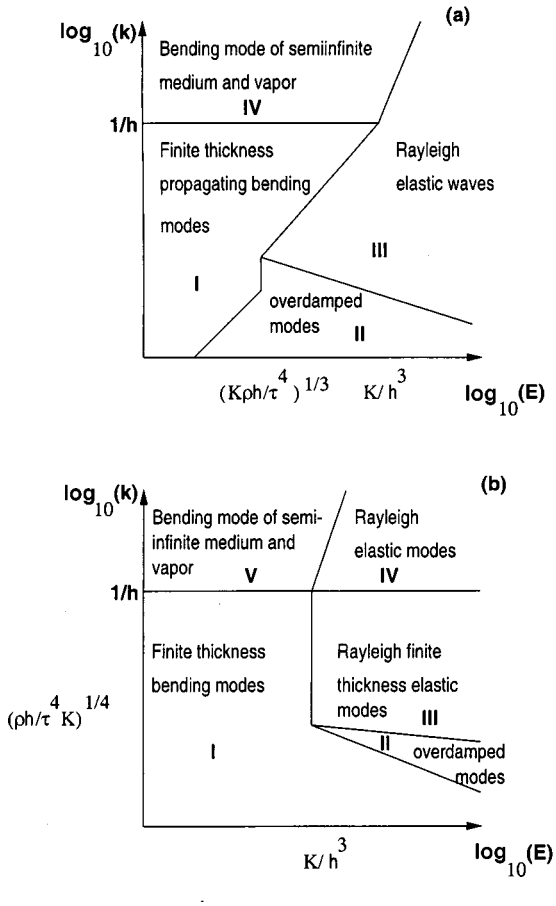

FIG. 2. Phase diagram of bending modes in terms of the wave vector k and the shear elastic modulus E for the squeezing (a) and undulation mode (b). The surface tension and interfacial elasticity are zero. The resonance frequencies in each region with their asymptotic boundary lines are explained in Sec. V.

Figure 2(b) depicts the undulatory mode phase diagram. At $w\tau<1$, region I corresponds to a finite-thickness propagating bending mode $w^2=Kk^4/2\rho h$ and the overdamped modes are $w=i\nu k^4h^2/3$ and $w=3iK/2\eta h^3$, which are located in region II with wave vector in the range $(K/\rho\nu^2h)^{1/4}<kh<1$. In the range of $kh<(K/\rho\nu^2h)^{1/4}<1$ there is an overdamped bending mode $w=iKk^2/2\eta h$. Finite-thickness Rayleigh modes $w^2=Ek^4h^2/3\rho$ are located in region III. In the short wavelength limit $hk>1$ and $w\tau<1$ the frequency of the finite thickness layer is dissipative $w=iKk^3/4\eta$. For $kh>1$, the semi-infinite medium with a single interface, there are a propagating bending mode $w^2=Kk^5/\rho$ in the limit, $w\tau<1$, and a Rayleigh elastic wave $w^2=4Ek^2/\rho$ for $w\tau>1$.

In a recent paper Buzza *et al*. [16] have considered the surface modes on a fluid-fluid interface with adsorbed poly-

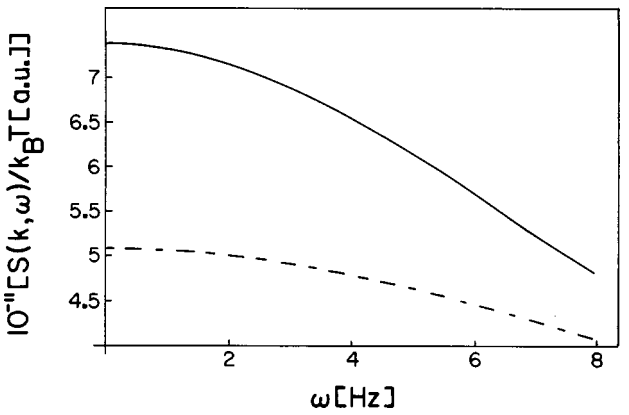

FIG. 3. Power spectrum of undulatory mode with inclusion of bending rigidity $K=k_BT$. The surface tension and interfacial elasticity are zero. Bulk shear elasticity $E=10$ N/m^2, $\tau=7.8\times10^{-6}$ sec (continuous line), $E=93$ N/m^2, $\tau=3.5\times10^{-5}$ sec, (dot-dashed line). In both cases the solvent viscosity is $\eta_s=6$ cP and the layer thickness $h=2\times10^{-6}$ m.

meric surfactants. Their model interface consists of a very thin diblock copolymer layer with elastic constants ϵ,γ,K and a real viscosity η_s, and a coupling parameter λ associated with the coupling of lateral compression and transverse deformation of the interface. Their expression of the elastic free energy for interface deformation is the same as our Eq. (2) in Sec. II for this quantity, with the basic difference being that they calculated an important contribution to this equation Eq. (2) due to the coupling term; $-\lambda\int_a(\partial\zeta/\partial x)^2(\partial^2\xi/\partial x^2)dS$.

For the special case of a thin liquid-liquid monolayer, λ can be neglected, and for an ultralow surface tension they predicted that the relaxation frequency of bending modes scales like $w\approx Kk^5/\rho$. In this limit of a very thin layer their model system and our model layer become equivalent when $\gamma=0=\epsilon$ and $h\to\infty$ (case of a single interface of a semiinfinite medium). In this case our calculation, using the dispersion relation of the undulatory mode [Eq. (22)] confirms this scaling relationship for the frequency as explained above. However, when the layer thickness is increased, the coupling term proportional to λ becomes more important and it cannot be neglected. Therefore, the effect of the lateral-transverse coupling on the undulation and squeezing modes [Eqs. (17) and (22)] for a finite-thickness layer should be taken into account. In Appendix C we provide the correct expressions for these modes when the coupling term is incorporated into the theory.

The effect of bending rigidity K in the power spectrum of scattered light is demonstrated in Fig. 3. For liquid monolayers with a dynamics described by the bending elastic energy of deformation $K\approx1k_BT-20k_BT$, the frequency range of the surface wave is $0-90$ Hz for a Newtonian solvent of shear viscosity $\eta_s=6$ cP, $\rho=10^3$ Kg/m^3, and layer size $h=2\times10^{-6}$ m, where the wave vector is $k=2\pi/h$. The continuous curve is the power spectrum in the case of a very small value of surface tension and with inclusion of bulk $E=10$ N/m^2 elasticity, $\tau=7.8\times10^{-6}$ sec and there is no interfacial ϵ elasticity in the long wavelength limit. In this case the spectral maximum is centered around zero frequency. When $E=93$ N/m^2, $\tau=3.5\times10^{-6}$ sec, the intensity is reduced by a factor of 4 with respect to the previous case as is shown in the dotted-dash curve. This reduction in the spectral intensity is due to the viscoelasticity response of the layer. In both cases studied the power spectra are broad, which mean that these bending modes are damped waves.

The power spectrum was studied at the characteristic modes of Fig. 2 and shows a quite similar shape in all cases as those illustrated in Fig. 3, with the maximum occurring at the frequencies predicted by the asymptotic relationships of Fig. 2.

We discuss now the power spectra as given by Eqs. (17)–(23) using the Maxwell model, and in the case that $K=0$ and γ and ϵ have a finite value. The dispersion relation of both modes, squeezing and undulatory modes [Eqs. (17) and (22)], shows a rather rich behavior of surface waves from the surface fluctuations. Therefore, to show the general trends of the spectra as obtained from the expressions of $S(k,w)$ let us focus first on the spectra of the squeezing modes (qualitatively similar conclusions are found for the undulatory mode) and limit our discussion to the low-frequency range $\omega\tau\ll1$ at which the viscous liquid behavior prevails. The next step will be the discussion of the high-frequency limit $\omega\tau\gg1$ or viscoelastic dynamic. Therefore, in order to cover all these different regimes we select conveniently as material parameters, for instance, those appropriate for poly (N-vinyl-2-pyrrolidone) with water as the solvent; solvent viscosity $\eta_s=1$ cP, surface tension $\gamma=72$ mN/m, effective medium density $\rho=10^3$ kg/m^3, degree of polymerization $N=10^4$, monomer size $a=1.8$ Å, polymer relaxation time τ, and interfacial elasticity $\epsilon=\alpha\gamma$ with α a constant and amplitude of wave vector $k=10\,000$ m^{-1}. We will neglect for simplicity of our analysis the contribution of the direct interactions (disjoining pressure $P_d=0$) and bending rigidity ($K=0$) to the surface dynamics. In the limit $w\tau<1$, $\eta(\omega)\approx E\tau+\eta_s$. If the surface elasticity is zero ($\epsilon=0$), the resonance frequencies, which scales, with the magnitude of the wave vector k are [14] a propagating capillary wave at $\omega^2=\gamma k^4h/2\rho$ for low values of the kinematic viscosity $\nu=\eta(w)/\rho$, and for moderate to high wave vector an overdamped capillary mode $w^2=i\gamma k^2h/8\eta$ and the viscous solution mode $w=i2\nu k^2$.

Typical spectra of Eq. (14) complemented with Eqs. (17)–(20) at the long wavelength limit $kh<1$ are shown in Fig. 4(a) for different amplitudes of the module of elasticity E and layer thickness $h=6.28\times10^{-6}$ m or equivalently $kh=0.02\pi$ with $\epsilon=0$. In Fig. 4(a) we show the frequency variation of the capillary peaks when the bulk shear elasticity E is increased. The two highest intensity peaks with E_1 and E_2 bulk modulus are capillary peaks of the type $w^2=\gamma k^4h/2\rho$. In the same Fig. 4(a) the more lower intensity peaks (E_3, E_4 and E_5) correspond to a capillary mode at a moderate wave vector in the viscous regime. It should be observed that these resonance peaks result from a combined effect of surface tension and bulk elasticity. Therefore, its nature is more of the second type of capillary wave mentioned just above ($w^2=i\gamma k^2h/8\eta$), and this fact can be observed if we go to a more concentrated solution and thus to a higher value of the amplitude of shear modulus as is shown there. It is observed in that plot that these capillary peaks become more intense, its linewidth sharpens, and their frequencies shift slightly to a lower value of frequency when E is increased as is predicted by the second algebraic relation-

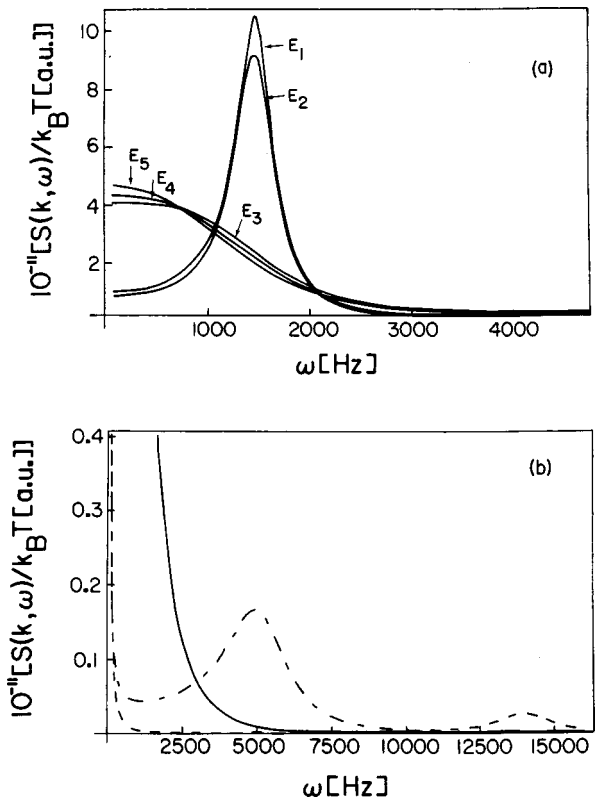

FIG. 4. Structure factor $S(k,w)$ of the squeezing mode in the viscous liquid regime, $w\tau<1$ and long wavelength limit $kh<1$ with $|qh|<1$. The wavelength is $k=10^4$ m^{-1} and the layer thickness $h=6.28\times10^{-6}$ m with material parameters $\rho=10^3$ kg/m^3, $\eta_s=1$ cP, $\gamma=72$ mN/m and interfacial elasticity $\epsilon=0$. Figure 4(a) with bulk shear elasticity $E_1=10$ N/m^2, $\tau_1=7.8\times10^{-6}$ sec and observed frequency $w_1=1.47\times10^3$ sec^{-1}, $E_2=20$ N/m^2, $\tau_2=1.2\times10^{-5}$ sec, $w_2=w_1$, $E_3=93$ N/m^2, $\tau_3=3.5\times10^{-5}$ sec, $w_3=867$ sec^{-1}, $E_4=110$ N/m^2, $\tau_4=3.8\times10^{-5}$ sec, $w_4=133$ sec^{-1}, $E_5=119$ N/m^2, $\tau_5=4.2\times10^{-5}$ sec, and $w_5=90.8$ sec^{-1}. In these plots the corresponding labels for each plot is assigned from top right (E_1) to the lower plot (bottom E_5). The plot labeled (b) only illustrates the effect of $\epsilon=0$ (continuous line), $\epsilon=0.01\gamma$ (dot-dashed) and $\epsilon=0.1\gamma$ (dashed line).

ship given above. It should be noticed also the effect that surface elasticity has on the spectra when its magnitude is increased as is shown in the dashed plots of Fig. 4(b) for a fixed E_5. Thus, for the moment let us study the effect of ϵ. When ϵ is increased gradually while keeping fixed E_5, the capillary peak decreases its intensity and moves to a higher frequency and broadens, and starts to develop a quasielastic peak located at a lower frequency, Fig. 4(b) (dot-dashed). Eventually, for a higher value of ϵ, Fig. 4(b) (dashed line), the quasielastic peak with a very small frequency becomes a monotonously decaying spectrum that has a small shoulder reminiscent of the capillary peak, which has shifted towards a higher value of frequency moving to the range of $\omega\tau>1$. Let us investigate now the effect of making the layer of the film thicker on the viscous regime $w\tau<1$. For this purpose let us consider the parameters of the situation of Fig. 4 (case $\epsilon=0,E_5$ only) and increase the thickness of the layer up to the limit where the two interfaces do not interact, i.e., of a single fluctuating monolayer, Fig. 5. In doing so we have

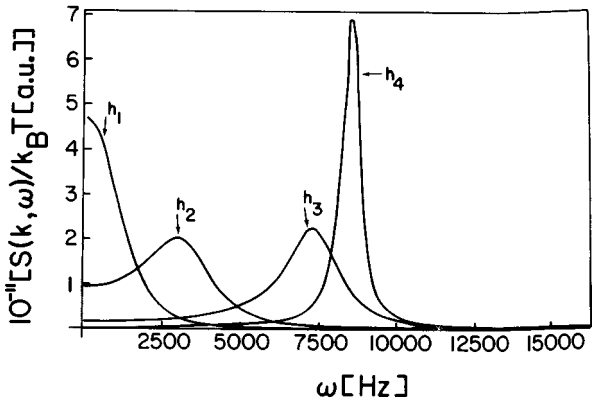

FIG. 5. $S(k,w)$ versus w of squeezing mode in the viscous liquid regime and long wavelength limit. The parameters considered are $k=10^4$ m^{-1}, $\rho=10^3$ kg/m^3, $\eta_s=1$ cP, $\gamma=72$ mN/m, $\epsilon=0$, $E=119$ N/m^2, and $\tau=4.2\times10^{-5}$ sec, for different layer thickness, $h_1=0.02\pi$/k, $h_2=0.3\pi$/k $h_3=0.6\pi$/k and $h_4=\infty$. The capillary peak (h_4) is $w_\gamma=8.5\times10^3$ sec^{-1}. Increasing thickness starts from the left side of frequency axes.

gone from the long wavelength limit (h_1), that is, length scales larger than the thickness of the layer towards one, which is a comparable length scale with respect to $h(h_4)$. It is observed that the capillary peak with $\epsilon=0$ (line with h_1 in Fig. 5) shifts to a higher value of frequency when h is increased (h_2 and h_3), but contrary to the cases in Fig. 4 it does not broaden but instead becomes sharper. Its intensity decreases first when the wavelength changes from long down to moderate; however, when the capillary peak is approached (short wavelength limit), the power spectrum intensity increases again up to a factor of 2 with respect to the peak of the initial capillary wave with E_5.

If we increase still more the thickness of the layer and go to the limit of a single fluctuating interface $kh\to\infty$ of a semi-infinite medium, the wave reaches the capillary mode $\omega_\gamma\to(\gamma k^3/\rho)^{1/2}$ that has the magnitude $\omega_\gamma\approx8.5\times10^3$ sec^{-1}, where we have used the values of γ, k, and ρ as given in Fig. 4. This value is in agreement with the one shown in the plot of Fig. 5 that was, however, obtained with the exact expression of $S(k,w)$ of Eq. (14) and Eqs. (17)–(20) in the single interface limit of a semi-infinite medium. It should be pointed out that the effect of interfacial elasticity is not relevant in this regime of wave vector $k\approx10^4$ m^{-1} and frequency $\omega\tau<1$, whenever $kh\to\infty$. This would be observed for a finite value of surperficial elasticity, for instance, $\epsilon=0.01\gamma$, where the capillary peak would have moved towards the frequency value of w_γ as in the case of $\epsilon=0$. Therefore, the capillary peak is exactly the same as in a single bare interface of a half-space geometry, $z<0$.

Thus we can draw the following important trends: at a moderate thickness of the layer such that we are within the range $kh<1$, and in the viscous liquid regime $\omega\tau<1$, the layer sustains a quasielastic wave around zero frequency mainly due to superficial elasticity, and two capillary waves; one is a function of the surface tension but is independent of the elastic modulus E while the other is due to both surface tension and bulk shear elasticity, and of type $w^2=\gamma k^2h/8\eta$ as observed in Fig. 4 for the wave vector and material parameters considered there, with the first occurring at a higher

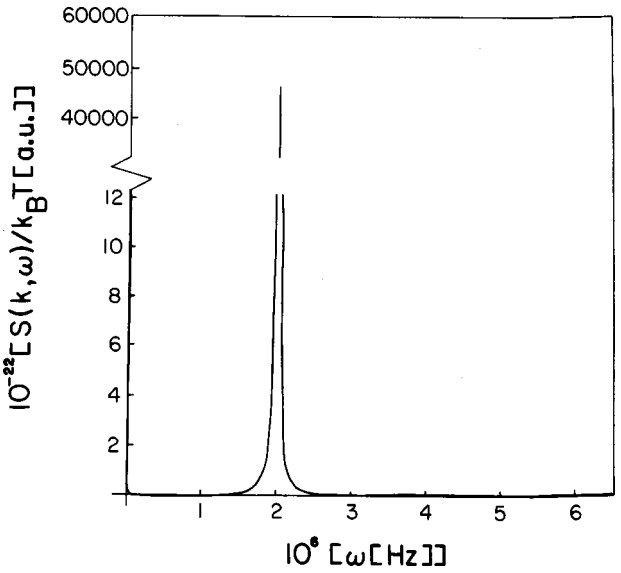

FIG. 6. Structure factor $S(k,w)$ of the squeezing mode in the elastic regime $w\tau>1$ and long wavelength limit $kh<1$ with $|qh|<1$, versus frequency w. The wavelength is $k=10^4$ m^{-1}, and the constant layer size $h=6.28\times10^{-6}$ m with material parameters $\rho=10^3$ kg/m^3, $\tau=1$ sec, $\eta_s=1$ cP, $\gamma=72$ mN/m, bulk shear elasticity $E=10^7$ N/m^2, and interfacial elasticity $\epsilon=0$. The observed elastic peak occurs at $w_e\approx2\times10^6$ sec^{-1} with $|qh|=0.1088$.

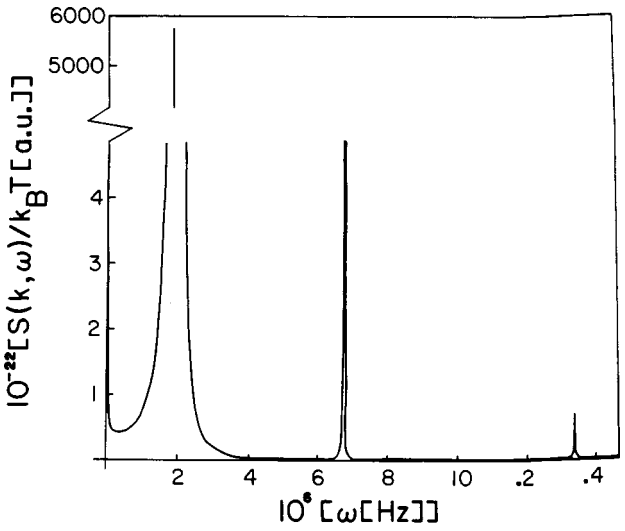

FIG. 7. Structure factor $S(k,w)$ of the squeezing mode in the elastic regime $w\tau>1$ at the threshold of the long wavelength limit $kh\approx0.942\,478$ and $|qh|\approx2.353\,2$ versus frequency w. The wavelength is $k=10^4$ m^{-1} and constant layer thickness $h=9.42\times10^{-5}$ m with material parameters $\rho=10^3$ kg/m^3, $\tau=1$ sec, $\eta_s=1$ cP, $\gamma=72$ mN/m bulk shear elasticity $E=10^7$ N/m^2, and two values of interfacial elasticity $\epsilon=0$ and $\epsilon=100\gamma$. The graphics with both values of ϵ merge in the single plot shown here, where the series of elastic peaks are of the order $w\approx10^6$ sec^{-1}.

strength of frequency. An increase in the thickness of the layer has, as a result, the capillary peaks shifting towards a single capillary peak afforded by surface tension only and remains as the only sustained mode of surface-roughness fluctuations and this situation is obtained when we have reached the limit of a single fluctuating membrane, Fig. 5.

If we return to Fig. 4 of a finite layer thickness $h=6.28\times10^{-6}$ m, $kh<1$ and $|qh|<1$ with $\epsilon=0$, and consider a high modulus of elasticity $E=10^7$ N/m^2, then we will cross over to the extreme elastic gel regime $\omega\tau>1$. Thus, the viscosity is frequency-dependent and given by $\nu=\nu_s+E/i\omega\rho$ and the dispersion relation, Eq. (17), predicts [14] a dissipative liquid mode $w=ik^2\nu_s$ and two propagating modes, a capillary one $w^2=\gamma k^4h/2\rho$ and a Rayleigh elastic wave $w_e^2=4Ek^2/\rho$, Fig. 6. In this case the Rayleigh wave has the same scaling relation as in the semi-infinite medium case and its magnitude as given by the last relation before is $w_e=2\times10^6$ sec^{-1} with $|qh|=0.1088$, a value that coincides with the one shown in Fig. 6 obtained with the exact expression of $S(k,w)$.

In the preceeding paragraph we have studied, in the long wavelength limit, $hk<1$ and $|qh|<1$ and high elastic regime, $w\tau>1$, the appearence of an elastic Rayleigh wave (Fig. 6). Since q is frequency dependent [Eq. (19)], it is possible to find surface waves in the long wavelength limit that satisfy $|qh|>1$ (Ref. [14]). The parameter $|qh|$ is well suited to describe a class of sustained surface waves that can be found in the dynamic description of the surface-roughness fluctuations on monolayer-covered viscoelastic films of finite thickness. In order to show those elastic modes let us increase the thickness of the layer starting from the one shown in the plot of Fig. 6 up to the threshold thickness $h=0.3\pi/k$ of long wavelength that satisfy $kh<1$ and amounts to the value $|qh|=2.3532$ which is already near the appearence of the elastic waves mentioned just above and for which $|qh|>1$ is satisfied. Figure 7 displays a train of several peaks of the power spectrum where, however, neither of them is of the Rayleigh type, w_e with $|qh|=0.1088$ described before. The different peaks shown in the plot of Fig. 7 are compressional elastic peaks afforded by the bulk elasticity E due to the increase in thickness of the layer and, therefore, by the availability of more accessible material to the thermal perturbation and their order can be estimated with Eq. (19) with the condition $w\tau>1$, from which results $w^2\approx(qh)^2E/\rho h^2$ and with the values of Fig. 7 gives $w\approx10^6$ sec^{-1}.

In the same plot the effect of a finite superficial elasticity is shown that however, leads to the same spectra; thus, this value of ϵ or even the extreme value case $\epsilon=100\gamma$ does not have an important effect on the spectra. It is possible that this train of elastic peaks is not observed in a real situation since they show only a very tiny intensity even after being amplificated several times. However, a careful analysis of the graphics of Fig. 7 and the set of parameter values at which those peaks have occurred suggest that if we increase even more the thickness of the layer they could display a more emphasized effect on the spectra. Thus, we increase still more the thickness of the layer. That is, we crossover from the limit $kh<1$ with $|qh|>1$ towards the elastic regime of moderate and short wavelength $kh>1$, with $|qh|>1$. In Fig. 8 we show a typical plot with the same parameter values as that in Fig. 7 but for a thicker layer with thickness $h=1.2\pi/k$ and using two different wavelengths; Fig. 8(a), $k=10\,000$ m^{-1}; and Fig. 8(b), $k=20\,000$ m^{-1}. Once again there appears a train of elastic peaks, all of which have a finite width with an enhanced strength of intensity as compared to those of Fig. 7. Longer wavelengths separate more

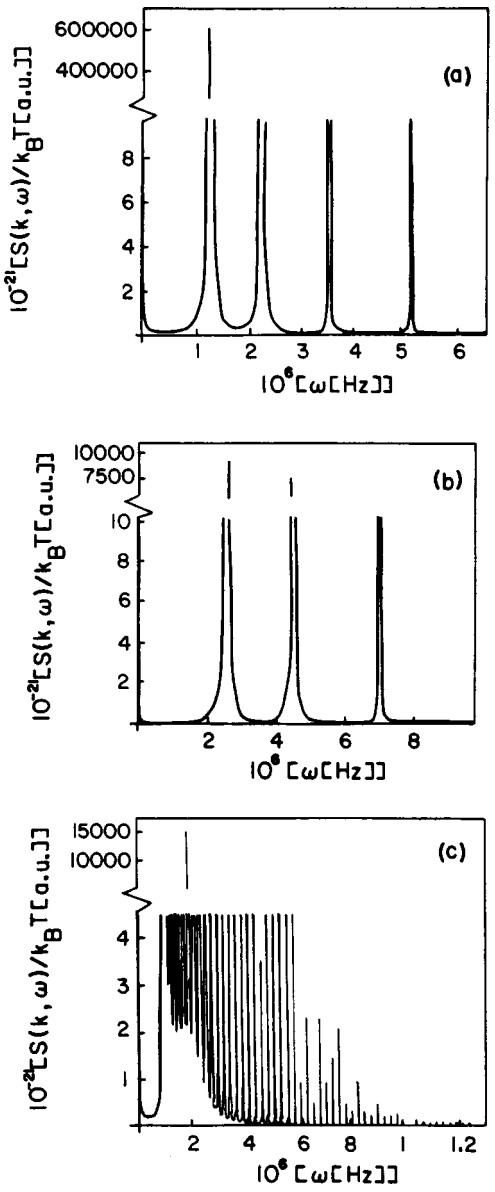

FIG. 8. Structure factor $S(k,w)$ versus frequency w of the squeezing mode in the elastic regime $w\tau>1$, moderate and large wavelength limit $kh>1$ and $|qh|>1$ with material parameters $\rho=10^3$ kg/m^3, $\tau=1$ sec, $\eta_s=1$ cP, $\gamma=72$ mN/m, interfacial elasticity $\epsilon=0$, and bulk shear elasticity $E=10^7$ N/m^2 at two different wavelengths. (a) $k=10^4$ m^{-1} with layer thickness $kh=1.2\pi$, (b) $k=2\times10^4$ m^{-1} with layer size $kh=1.2\pi$, and (c) $k=10^4$ m^{-1} for the infinitely thick layer case $h\to\infty$. In the cases of (a) and (b) the order of the first resonance frequency peak is $w\approx10^6$ sec^{-1}.

the resonance frequency peaks as is shown in Fig. 8(b). This clearly defined sequence of almost equally spaced peaks is shown only in the range of layer thickness $h=0.2\pi\beta/k$ with $1\leqslant\beta\leqslant8$ for the parameters considered in those plots. For the larger thickness and in the limit of a single covered monolayer $h\to\infty$ all the peaks diminish its intensity, narrow, and merge to the profile of a single quasielastic broad peak as is shown in Fig. 8(c). This train of peaks displayed just above in the plot of the power spectrum $S(k,w)$, were, in fact, predicted by Sens *et al.* (Ref. [14]) for a finite-thickness layer of a homogeneous polymeric liquid where the viscous properties of the solvent were neglected. The interfaces of the polymer layer were characterized by the elastic constants γ and ϵ. They provided the strength of the corresponding frequencies of the sustained modes on the layer through an analysis of approximate expressions of the dispersion relations. In our present paper we have taken into account the solvent properties and another elastic quantity, the bending rigidity modulus K, which turns out to be relevant in the dynamics of a wide class of polymeric surfactant monolayers. In this paper we provide the full expressions of the power spectrum $S(k,w)$ and their analysis, and of the dispersion relations for the two main collective modes, squeezing and undulatory, which under the limits considered by Sens *et al.* [14] reduce to their results for the dispersion relations when $K=0$, $\eta_s=0$, and $\rho_s=0$.

VI. CONCLUSION

We have provided the dispersion relations and power spectra of the squeezing and undulatory modes of a freely standing layer of a viscoelastic material using the two-fluid model. An asymptotic analysis of the dispersion equation provides expressions of the characteristic bending modes, which consist of propagating and overdamped bending modes to Rayleigh elastic waves. Figure 3 demostrates that bulk elastic properties of the polymer layer produces a lower intense spectrum than the layer constituted by a simple Newtonian nonviscoelastic fluid for finite K and negligible surface tension and interfacial elasticity. In the opposite situation of zero-bending energy K, we have shown that in the elastic regime and for a wavelength comparable to the thickness of the layer (that is, short and moderate wavelengths $kh>1$ and $|qh|>1$), the power spectrum displays a series of peaks associated with elastic waves whose resonance frequencies are due to the bulk shear elasticity E of the underlying polymer network. At these values of E, surface elasticity ϵ produces effectively a negligible effect on the spectra $S(k,w)$ even at extreme values of $\epsilon=100\gamma$. It is possible to find the same class of elastic peaks in the long wavelength range $kh<1$, $|qh|>1$; however, almost all of them are a tiny effect. For lower values of the amplitude of bulk elasticity E, that is, in the case of low and moderately concentrated polymer solutions, surface elasticity ϵ starts to play an important role shifting the magnitude of the present resonance peaks and producing in all cases studied, a monotonously quasielastic peak around zero frequency (Fig. 4). Our general and exact expressions of the structure factor, Eqs. (20) and (21), reduce to the equivalent properties of a single fluctuating monolayer of the semi-infinite medium, Eq. (24), in the limit of noninteracting interfaces of the layer $h\to\infty$. Since our model of the viscoelastic layer consists of surface-active interfaces characterized by ϵ, γ, P_d, and bending rigidity K, in the limit ($h\to\infty$) of an elastic monolayer, our expression of the dispersion relation generalizes those reported previously for the two-fluid model of a single viscoelastic interface. Thus, Eqs. (20), (21), and (24) may be useful to describe the superficial hydrodynamic properties of a viscoelastic surfactant membrane where bending rigidity is the most relevant energy scale of the interface, and surface tension is a negligible effect.

ACKNOWLEDGMENTS

This work was supported by the MRL program of the National Science Foundation under Award No. DMR96-32716 and by STEPI, Korea. M.H.C. also acknowledges support from Conacyt Mexico through Grant No. 26270-E.

APPENDIX A

We demonstrate in this appendix that Eq. (25) is equivalent to the dispersion relation of Wang *et al.* (Eq. (46) of Ref. [12]),

$$D(w)=-\Gamma^2\sqrt{1+\frac{2iw}{\Gamma}}+(iw+\Gamma)^2+w_\gamma^2 + w_\epsilon^2\left[w_\gamma^2\left(1-\sqrt{1+\frac{2iw}{\Gamma}}\right)\Big/\ w^2+\sqrt{1+\frac{2iw}{\Gamma}}\right], \tag{A1}$$

where $w_\gamma=(\gamma k^3/\rho)^{1/2}$, $w_\epsilon=(\epsilon k^3/\rho)^{1/2}$, and $\Gamma=2\nu k^2$. Using the above quantities, Eq. (A1) can be written as

$$D(w)=-4k^4\nu^2\sqrt{1+\frac{iw}{\nu k^2}}+(iw+2k^2\nu)^2+\frac{\gamma k^3}{\rho} + \frac{\epsilon k^3}{\rho}\left[\frac{\gamma k^3}{\rho w^2}\left(1-\sqrt{1+\frac{iw}{\nu k^2}}\right)+\sqrt{1+\frac{iw}{\nu k^2}}\right]. \tag{A2}$$

Using now the identity $q=k\sqrt{1+iw/\nu k^2}$ in Eq. (A2),

$$D(w)=\frac{4k^4\nu^2 q}{k}+(iw+2\nu k^2)^2+\frac{\gamma k^3}{\rho} + \frac{\epsilon k^3}{\rho}\left[\frac{\gamma k^3}{\rho w^2}\left(\frac{k-q}{k}\right)+\frac{q}{k}\right]. \tag{A3}$$

Multiplying both sides of Eq. (A3) with $-w^2$ results in

$$-w^2D(w)=(-w^2+2i\nu k^2 w)^2 - w^2\left(\frac{\gamma k^3}{\rho}+\frac{\epsilon q k^2}{\rho}-4\nu^2k^3q\right) + \frac{\epsilon k^2}{\rho}(q-k)\frac{\gamma k^3}{\rho}, \tag{A4}$$

which is Eq. (25) with $K=0$.

APPENDIX B

Here we demonstrate that the Lucassen and Lucassen-Reynders [19] result is equivalent to Eq. (25). The generalized Lucassen equation reads

$$\left(\frac{\epsilon k^2+Kk^4}{w}+i\eta(k+q)\right)\left(\frac{\gamma k^2+Kk^4}{w}-\frac{w\rho}{k}+i\eta(k+q)\right) + [\eta(k-q)]^2=0, \tag{B1}$$

We expand this equation and multiply it by the factor $(q-k)w^2k$, and use the identity $-\eta^2(k+q)^2+\eta^2(k-q)^2=-4kq\eta^2$, thus, Eq. (B1) can be written

$$(q-k)\epsilon k^2(\gamma k^2+Kk^4)k-\epsilon k^2\rho w^2(q-k) + \epsilon k^3 i\eta(k+q)(q-k)w+(\gamma k^2+Kk^4)i\eta kw \times(q+k)(q-k)-i\eta\rho w(q+k)(q-k)w^2 - 4\eta^2k^2qw^2(q-k)=0. \tag{B2}$$

Using now the identities $(q+k)(q-k)=q^2-k^2$ and $q^2-k^2=iw/\nu$ in Eq. (B2), and dividing this equation by ρ^2 we get, after some algebraic steps,

$$w^4-w^2\left(\frac{\gamma k^3+Kk^5}{\rho}+\frac{\epsilon k^2 q}{\rho}\right)+\frac{\epsilon k^3w^2}{\rho}-\frac{\epsilon k^3w^2}{\rho} + \frac{\epsilon k^2}{\rho}\left(\frac{\gamma k^3+Kk^5}{\rho}(q-k)\right)-4\nu^2k^2qw^2(k-q)=0. \tag{B3}$$

Since the term $-4k^2\nu^2qw^2(k-q)=-4k^4\nu^2w^2-4i\nu k^2w^3+4k^3\nu^2qw^2$ where we used the identity $q^2=k^2+iw/\nu$, we rewrite Eq. (B3) as

$$w^4-4i\nu k^2w^3-4\nu^2k^4w^2-w^2\left(\frac{\gamma k^3+Kk^5}{\rho}+\frac{\epsilon qk^2}{\rho} - 4\nu^2k^3q\right)+\frac{\epsilon k^2}{\rho}(q-k)\frac{\gamma k^3}{\rho}=0 \tag{B4}$$

or

$$(-w^2+2i\nu k^2w)^2-w^2\left(\frac{\gamma k^3+Kk^5}{\rho}+\frac{\epsilon qk^2}{\rho}-4\nu^2k^3q\right) + \frac{\epsilon k^2}{\rho}(q-k)\left(\frac{\gamma k^3+Kk^5}{\rho}\right)=0, \tag{B5}$$

which is Eq. (25).

APPENDIX C

In order to include into the dispersion relations of the squeezing and undulatory modes, Eqs. (17) and (22), the effect of the lateral-transverse coupling λ, we consider as new boundary conditions equivalent to Eqs. (10) and (11); for the balance force in the normal direction,

$$p^0=p_s+\gamma\frac{\partial^2\xi}{\partial x^2}+K\frac{\partial^4\xi}{\partial x^4}-P_d'(h)\,\delta\xi+2\eta\frac{\partial v_z}{\partial z}+\lambda\frac{\partial^3\zeta}{\partial x^3} \tag{C1}$$

at $z=0$, and for the tangential forces the boundary condition reads

$$\sigma_{zx}=\epsilon\frac{\partial^2\zeta}{\partial x^2}-\lambda\frac{\partial^3\xi}{\partial x^3},\quad z=\pm\frac{h}{2}. \tag{C2}$$

From these boundary conditions, Eqs. (C1) and (C2), the resulting dispersion relations are for the squeezing mode,

$$D^s_\lambda(k,w)=D^s(k,w)+\left(\frac{4ik^5\nu\lambda w}{\rho}-\frac{k^7\lambda^2}{\rho^2}\right)\tanh\left(\frac{hk}{2}\right)\times\left[q\coth\left(\frac{hq}{2}\right)-k\coth\left(\frac{hk}{2}\right)\right]+\frac{2w^2\lambda k^4}{\rho}, \tag{C3}$$

and for the undulatory mode,

$$D^u_\lambda(k,w)=D^u(k,w)+\left(\frac{4ik^5\nu\lambda w}{\rho}-\frac{k^7\lambda^2}{\rho^2}\right)\coth\left(\frac{hk}{2}\right)\times\left[q\tanh\left(\frac{hq}{2}\right)-k\tanh\left(\frac{hk}{2}\right)\right]+\frac{2w^2\lambda k^4}{\rho}, \tag{C4}$$

where $D^s(k,w)$ and $D^u(k,w)$ are Eqs. (17) and (22) respectively. The relaxation function χ that appears in $S(k,w)=(k_BT/\pi w)\mathrm{Im}[\chi]$ remains exactly the same as given in Eqs. (20) and (21) where it is only necessary to replace $D^s(k,w)$ by $D^s_\lambda(k.w)$ and $D^u(k,w)$ by $D^u_\lambda(k,w)$. The limit $h\to\infty$ reads

$$D^{sin}_\lambda(k,w)=D_{sin}(k,w)+\left(\frac{4ik^5\nu\lambda w}{\rho}-\frac{k^7\lambda^2}{\rho^2}\right)(q-k)+\frac{2w^2\lambda k^4}{\rho}. \tag{C5}$$

[1] *Light Scattering by Liquid Surfaces and Complementary Techniques*, edited D. Langevin, Surfactant Science Series (Dekker, New York, 1992).
[2] F. Monroy, F. Ortega, and R.G. Rubio, Phys. Rev. E **58**, 7629 (1998).
[3] J.C. Earnshaw, Adv. Colloid Interface Sci. **68**, 1 (1996).
[4] *Liquids at Interfaces*, Proceedings of the Les Houches Summer School, edited by J. Charvolin, J.F. Joanny, and J. Zinn-Justin (North Holland, Amsterdam, 1990).
[5] in *Structure and Dynamics of Membranes*, edited by R. Lipowsky and E. Sackman (Elsevier North Holland, Amsterdam, 1995).
[6] P. Krindel and A. Silberberg, J. Colloid Interface Sci. **71**, 39 (1979).
[7] Q.R. Huang, C.H. Wang, and N.J. Deng, J. Chem. Phys. **108**, 3827 (1998).
[8] R.B. Dorshow and L.A. Turkevich, Phys. Rev. Lett. **70**, 2439 (1993).
[9] M.W. Kim, Colloids Surf., A **128**, 145 (1997).
[10] J.L. Harden, H. Pleiner, and P.A. Pincus, J. Chem. Phys. **94**, 5208 (1991).
[11] H. Nakanishi and S. Kubota, Phys. Rev. E **58**, 7678 (1998).
[12] C.H. Wang and Q.R. Huang, J. Chem. Phys. **107**, 5898 (1997).
[13] J.L. Harden and H. Pleiner, Phys. Rev. E **49**, 1411 (1994).
[14] P. Sens, C. Marques, and J.F. Joanny, Langmuir **9**, 3212 (1993).
[15] V. Kumaran, J. Chem. Phys. **98**, 3429 (1993).
[16] D.M.A. Buzza, J.L. Jones, T.C.B. McLeish, and R.W. Richards, J. Chem. Phys. **109**, 5008 (1998).
[17] J. Meunier and L.T. Lee, Langmuir **7**, 1855 (1991).
[18] S.A. Safran, *Statistical Mechanics of Surfaces, Interfaces, and Membranes* (Addison Wesley, Reading, MA, 1994).
[19] J.L Lucassen and E.H. Lucassen-Reynders, Adv. Colloid Interface Sci. **2**, 347 (1969).
[20] J.G.H. Joosten, J. Chem. Phys. **80**, 2383 (1984).
[21] P.G. de Gennes, Macromolecules **9**, 587 (1976).
[22] L.D. Landau and E.M. Lifshitz, *Fluid Mechanics* (Pergamon, New York, 1959).
[23] V. Levich, *Physicochemical Hydrodynamics* (Prentice Hall, Englewood Cliffs, NJ, 1962).